Polarization matching design of InGaN-based semi-polar quantum wells—A case study of $(11\bar{2}2)$ orientation

Grzegorz Kozlowski, Stefan Schulz, and Brian Corbett

Citation: Appl. Phys. Lett. **104**, 051128 (2014); doi: 10.1063/1.4864478
View online: http://dx.doi.org/10.1063/1.4864478
View Table of Contents: http://aip.scitation.org/toc/apl/104/5
Published by the American Institute of Physics

Polarization matching design of InGaN-based semi-polar quantum wells—A case study of (11$\bar{2}$2) orientation

Grzegorz Kozlowski,[a] Stefan Schulz, and Brian Corbett
Tyndall National Institute, Lee Maltings, Cork, Ireland

(Received 23 December 2013; accepted 25 January 2014; published online 7 February 2014)

We present a theoretical study of the polarization engineering in semi-polar III-nitrides heterostructures. As a case study, we investigate the influence of GaN, AlGaN, and AlInN barrier material on the performance of semi-polar (11$\bar{2}$2) InGaN-based quantum wells (QWs) for blue (450 nm) and yellow (560 nm) emission. We show that the magnitude of the total built-in electric field across the QW can be controlled by the barrier material. Our results indicate that AlInN is a promising candidate to achieve (i) reduced wavelength shifts with increasing currents and (ii) strongly increased electron-hole wave function overlap, important for reduced optical recombination times. © *2014 AIP Publishing LLC*. [http://dx.doi.org/10.1063/1.4864478]

In recent years, III-nitrides, such as InN, GaN, AlN and their respective alloys, have attracted considerable interest since their direct band gaps span, in principle, over the whole visible spectral range. This makes them ideal candidates for optoelectronic devices, such as light emitting diodes (LEDs) and laser diodes (LDs).[1] In particular, InGaN-based quantum wells (QWs) grown on *c*-plane GaN received much attention. However, a main drawback in realizing high performance devices based on *c*-plane nitride heterostructures is the inherent electrostatic built-in fields giving rise to a spatial separation of electron and hole wave functions in the active region.[2] Consequently, the radiative recombination rate is significantly decreased. Moreover, due to the screening of the built-in fields, *c*-plane nitride-based optoelectronic devices show a large emission wavelength shift for typical operating currents.[3–5] This shift is larger for LEDs emitting in green and yellow spectral regimes.

Several different approaches have been discussed in the literature to diminish the detrimental effect of these built-in fields. When using conventional *c*-plane substrates, the growth of quantum dots instead of QWs[6,7] or polarization matching between QW and barrier material[8,9] has been suggested and used. In addition, the growth on non- and semi-polar substrate orientations was applied to eliminate or reduce the electrostatic built-in fields.[10–13] For example, as shown by Zhao *et al.*,[14,15] the reduction of the electric field inside the active region can be more effective for particular semi-polar crystallographic orientations. Zhao *et al.* investigated structures grown on (20$\bar{2}$1) and (20$\bar{2}\bar{1}$) planes and showed that LEDs with superior emission characteristic can be achieved using the (20$\bar{2}\bar{1}$) orientation. It is important to note, that the built-in electric field, the optimal growth conditions, and the In incorporation differs for each semi-polar plane.

In this paper, we show that the QW emission can be optimized for a chosen semi-polar orientation. We utilize polarization matching between the QW and the barrier to reduce the built-in field in LEDs designed for operation in blue (450 nm) and yellow (560 nm) spectral regimes. More specifically, we investigate the semi-polar (11$\bar{2}$2) orientation, known for a very high indium incorporation,[16] and design InGaN-based LED structures with GaN, AlGaN, and AlInN barrier layers. We show that AlInN is a promising barrier material candidate to be used in high performance LEDs. The designed InGaN/AlInN structures show large carrier wave function overlap and improved color stability, i.e., reduced wavelength shift with increasing currents. In addition, the composition of the active region as well as the barrier can be tuned to further improve the device performance at a given current density. Although shown for a particular semi-polar orientation, the method of polarization matching presented here can be used in general for any growth plane.

Our calculations use the commercial SiLENSe package[17] based on a one-dimensional drift-diffusion model and including specific features of the nitride materials, e.g., strong electrostatic built-in fields arising from spontaneous and piezoelectric polarization. To take the effect of strain on the band edges into account, we first perform our own strain dependent $\mathbf{k}\cdot\mathbf{p}$ calculations and derive strain dependent band offsets. A similar approach including strain effects has recently been used by Zhao *et al.*[14,15] In addition, it has been highlighted by different groups that the band gap bowing parameter in InGaN[18,19] and even more pronounced in AlInN[20,21] shows a strong composition dependence. To account for this, we include in the model composition dependent band gap bowing parameters obtained from atomistic tight-binding supercell calculations, which show a very good agreement over the whole composition range with experimental data on InGaN[19] and AlInN[21] alloys.

We use as a model structure a 3 nm thick InGaN single QW sandwiched between 10 nm thick barriers and p- and n-doped GaN layers as shown schematically in Fig. 1. We focus on GaN, AlGaN, and AlInN as the barrier material. Although AlInN with 18% In is lattice matched to *c*-plane GaN, it is not fully lattice matched to the semi-polar (11$\bar{2}$2) orientation. For an accurate modelling and design of the active region of an LED structure, strain effects are of central importance, given the large lattice mismatch between the well and the barrier material. However, when assuming AlInN barrier layers which are almost lattice matched to the

[a]Electronic mail: grzegorz.kozlowski@tyndall.ie

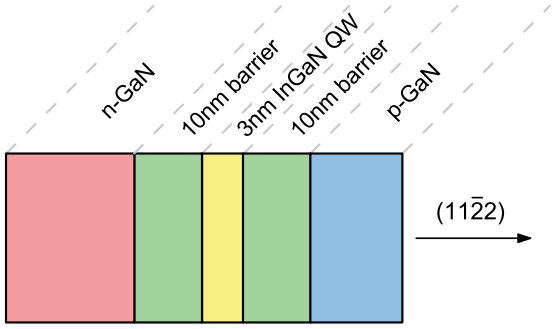

FIG. 1. Schematic illustration of a modelled LED structure.

underlying GaN, strain effects are of secondary importance. For the sake of a simplified discussion, we neglect the impact of the strain on the band edges in the AlInN barrier layer region and account for their composition dependent bowing only. Given that we focus on AlInN with 20% In, in comparison to the active region, this approximation should be well justified. The composition of the AlGaN barrier with 10% of Al was chosen to match the band gap of the studied AlInN layer which is 3.53 eV at room temperature. Since the band gap of the reference GaN is around 100 meV smaller, both AlInN and AlGaN barriers should provide slightly stronger confinement of carriers inside the QW. We start the discussion with the analysis of the built-in electric fields across the QW with three different barrier materials.

It is well known that semi-polar QWs still exhibit electrostatic built-in fields, arising from orientation dependent spontaneous and piezoelectric polarization.[22] The total built-in potential φ_{tot} across the QW is given by[9]

$$\varphi_{tot}(z) = \varphi_{sp}(z) + \varphi_{pz}(z) = \left\{\frac{(P_{sp}^{QW} - P_{sp}^{QB}) + P_{pz}^{QW}}{2\varepsilon_0\varepsilon_r^{QW}}\right\}\left(|z| - \left|z - \frac{h}{2}\right|\right), \quad (1)$$

where P_{sp}^{QW} and P_{sp}^{QB} are the spontaneous polarization of, respectively, the QW and the barrier, P_{pz}^{QW} is the piezoelectric polarization of the QW, h is the QW thickness with interfaces at $z = -h/2$ and $z = h/2$, ε_r^{QW} is the QW dielectric constant, and ε_0 is the vacuum permittivity. The drop of built-in electric potential $\Delta\varphi_{tot}$ across the QW defines the strength of the spatial separation of electrons and holes and, thus, the efficiency of optical recombination. In consequence, small and large $\Delta\varphi_{tot}$ corresponds to, respectively, high and low electron-hole wave function overlap $|\langle\psi_e|\psi_h\rangle|^2$. Both spontaneous and piezoelectric contributions can effectively reduce $\Delta\varphi_{tot}$, provided φ_{sp} and φ_{pz} are of opposite signs and comparable in magnitude. The quantities φ_{sp}, φ_{pz}, and φ_{tot} across an $In_{0.17}Ga_{0.83}N$ QW for GaN, AlGaN, and AlInN barrier materials in the semi-polar (11$\bar{2}$2) orientation are shown in Fig. 2. In the InGaN/GaN case, φ_{tot} is dominated by the piezoelectric polarization potential φ_{pz}. However, a small amount of Al in the barrier layer results in a much stronger φ_{sp} which is of opposite sign to φ_{pz} (see Fig. 2(b)). This increase of φ_{sp} is due to the fact that the spontaneous polarization in AlN is roughly two times larger than in GaN.[19] Although the φ_{sp} contribution is much smaller than the piezoelectric part for the studied composition, further optimization of the AlGaN layer will reduce $\Delta\varphi_{tot}$ and improve the wave function overlap inside the active region.

In comparison to systems with GaN and AlGaN barriers, for the InGaN/AlInN structure, $\Delta\varphi_{tot}$ is of opposite sign as shown in Fig. 2(c). Here, φ_{sp} is roughly twice as large as φ_{pz} due to a much higher AlN content. The important implication is that $\Delta\varphi_{tot}$ across the QW with the AlInN barrier layer can be substantially reduced and be eliminated by using an InGaN QWs with higher In content. For this case, the piezoelectric contribution will increase, therefore φ_{sp} and φ_{pz} will cancel each other by polarization matching. In Fig. 3, we present $\Delta\varphi_{tot}$ along the growth direction for the studied barriers as a function of the In content in the QW. Due to the small spontaneous polarization in the case of GaN and AlGaN, $\Delta\varphi_{tot} < 0$ for all InGaN QWs compositions. The situation for InGaN/AlInN is more complicated. For InGaN QWs with ~29% In, the system is polarization matched ($\Delta\varphi_{tot} = 0$). After taking the external potential of the p-n junction and the applied bias into account, our simulations indicate that at 10 A/cm^2 the optimal QW composition for which $\Delta\varphi_{tot} = 0$ corresponds to 23% In. Any variation from

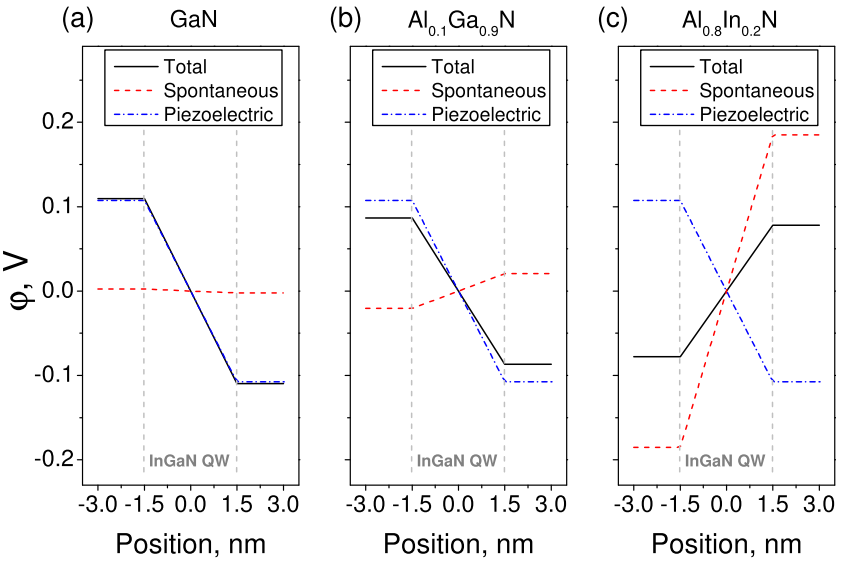

FIG. 2. Spontaneous, piezoelectric, and total built-in potential across the $In_{0.17}Ga_{0.83}N$ QW along the growth direction for structures with (a) GaN, (b) $Al_{0.1}Ga_{0.9}N$, and (c) $Al_{0.8}In_{0.2}N$ barriers.

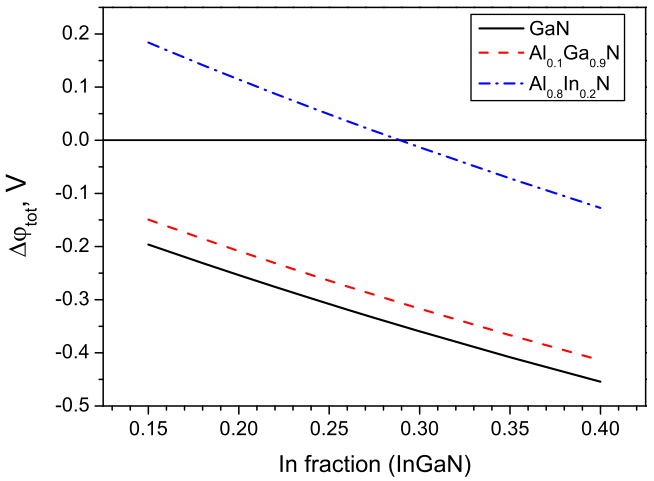

FIG. 3. Drop of total built-in electric potential within the QW along the growth direction for structures with GaN, AlGaN, and AlInN barrier layers as a function of InGaN composition.

this composition results in a non-zero drop of the potential across the active region and an increased spatial separation of the charge carriers in the QW. As a result, for the QW with In $< 23\%$, $|\Delta\varphi_{tot}|$ decreases with an increasing InN content. Therefore, a larger wave function overlap, and a more efficient LED is expected for a QW with a higher In content. On the other hand, for the QW with In $> 23\%$, $|\Delta\varphi_{tot}|$ increases and thus $|\langle\psi_e|\psi_h\rangle|^2$ decreases with an increasing In content similar to designs with GaN and AlGaN barriers.

We next focus our discussion on the simulation of LEDs containing the three different barrier materials. First, we consider an LED designed for blue emission at 450 nm corresponding to an InGaN QW with 17% In. Here, we focus on the emission characteristic and the carrier wave function overlap. A detailed analysis of the internal quantum efficiency droop phenomena widely discussed in the literature[8,23,24] is beyond the scope of the present study. Figure 4(a) displays the simulated electroluminescence (EL) emission wavelength as a function of the current density and for

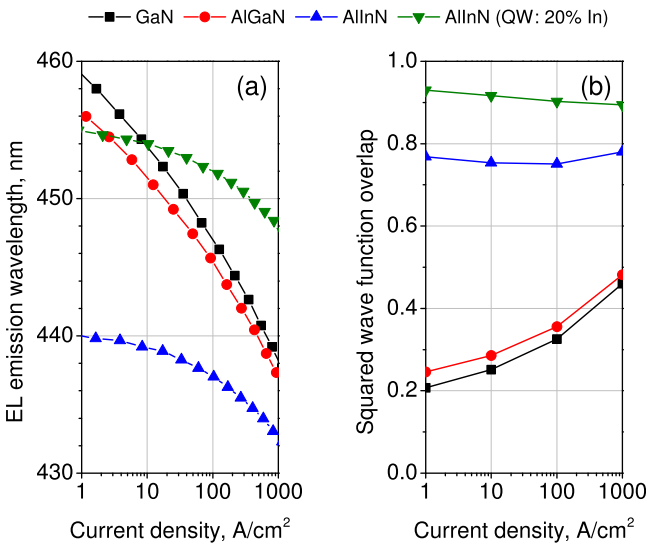

FIG. 4. $In_{0.17}Ga_{0.83}N$-based LED designed for blue emission (450 nm): Simulated EL emission wavelength (a) and squared electron-hole wave function overlap (b) for structures containing GaN, AlGaN, and AlInN barriers.

structures with different barrier materials (GaN, AlGaN, and AlInN). Using GaN and AlGaN as barrier layers results in a large shift of the emitted light from 455 nm at 1 A/cm^2 to 435 nm at 1000 A/cm^2. The structure containing AlInN, on the other hand, behaves significantly different. The shift of the emitted light is much smaller and is less than 10 nm in the presented current range. The overall emission wavelength is, however, lower and is 440 nm at 10 A/cm^2. In order to compensate for this blue shift, the In content of the QW was raised from 17% to 20%. As it can be seen, the emission wavelength shift is not increased and is still smaller than that of structures with GaN and AlGaN barriers. In addition to the strongly reduced wavelength shift in the LED structure with an AlInN barrier, we find also that $|\langle\psi_e|\psi_h\rangle|^2$ is strongly increased compared to systems with GaN and AlGaN barriers as shown in Fig. 4(b). For structures with GaN and AlGaN barriers, we calculated values of 20%–50% for 1 and 1000 A/cm^2, respectively, while for the InGaN/AlInN structures, $|\langle\psi_e|\psi_h\rangle|^2$ is larger than 70% over the current range. As already discussed, when increasing the InN content in the QW from 17% to 20%, the large spontaneous potential of the AlInN barrier is balanced by an increasing piezoelectric potential across the active region. As a consequence, $\Delta\varphi_{tot}$ is lowered, and the wave function overlap is further increased up to $\sim$90% for the QW with 20% In.

Although the magnitude of $\Delta\varphi_{tot}$ across the QW shown in Fig. 2 is comparable for all studied barriers, a much higher wave function overlap is calculated for the InGaN/AlInN system (Fig. 4(b)). This is due to the additional external electric potential which adds to φ_{pz} and therefore increases $\Delta\varphi_{tot}$ for the structures containing GaN and AlGaN barriers where $\varphi_{sp} \ll \varphi_{pz}$. However, due to a much larger spontaneous polarization contribution in AlInN, $\Delta\varphi_{tot}$ is decreased by the external potential in the InGaN/AlInN structure ($\varphi_{sp} > \varphi_{pz}$). Therefore, depending on the barrier material, the external potential can be used to reduce or to increase the electric field across the InGaN QW at a given current density. These features are presented in Figs. 5(a) and 5(b) where we show the valence band structure for designs with, respectively, GaN and AlInN barriers at 10 A/cm^2. In addition to a smaller $|\langle\psi_e|\psi_h\rangle|^2$, the large value of $\Delta\varphi_{tot}$ for the InGaN/GaN and the InGaN/AlGaN cases results in strong localization of holes at one side of the QW (Fig. 5(c)). This in turn results in an emission at longer wavelength compared to the InGaN/AlInN system shown in Fig. 4(a). For increasing current density, the electric potential across the QW is screened and large emission wavelength shift together with an increased wave function overlap is calculated.

We next discuss the results of LEDs emitting in the yellow spectral regime. In order to realize emission at 560 nm, the In content in the QW is increased to 31%. The simulated EL emission wavelength for structures with the three different barrier materials is presented in Fig. 6(a). The emission wavelength of the InGaN/AlInN LED is blue shifted by more than 20 nm with respect to the other barrier designs. As a consequence, the In content in the QW has to be increased up to 36% to achieve yellow emission. Similar to the blue LED, structures with the AlInN barriers show superior emission behaviour, e.g., a wavelength shift smaller than 20 nm due to the reduced electric field. Structures with GaN and

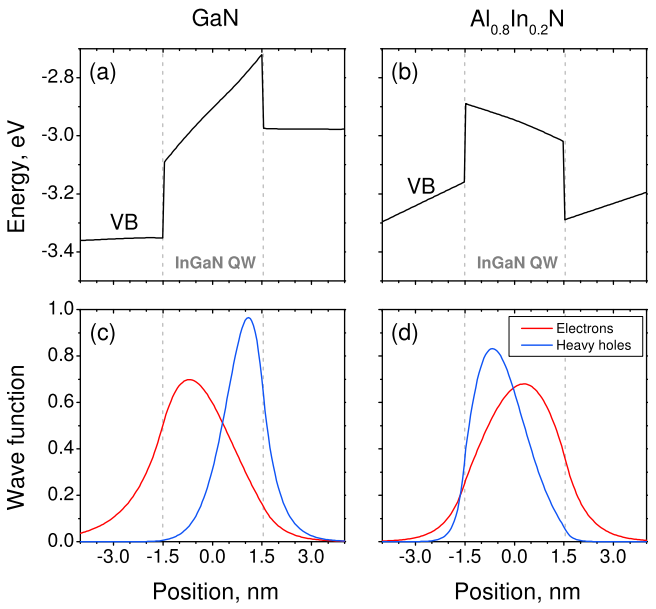

FIG. 5. Valence band structure (top) and electron and heavy hole wave functions (bottom) for $In_{0.17}Ga_{0.83}N/GaN$ and $In_{0.17}Ga_{0.83}N/Al_{0.8}In_{0.2}N$ at 10 A/cm^2 (~2.85 V).

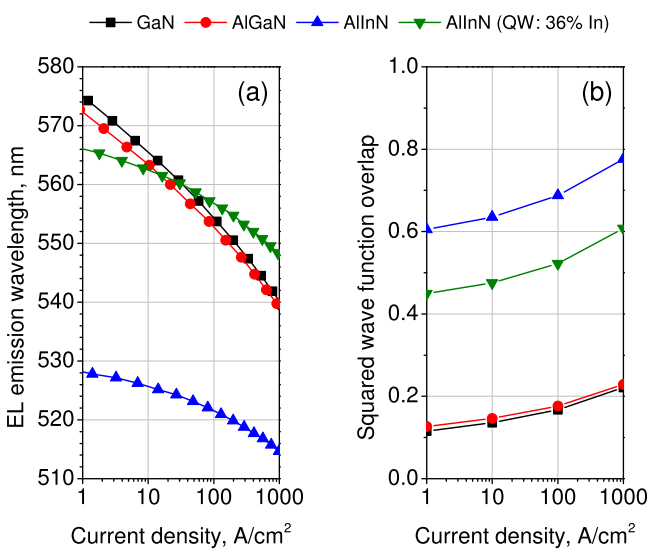

FIG. 6. $In_{0.31}Ga_{0.69}N$-based LED designed for yellow emission (560 nm): Simulated EL emission wavelength (a) and squared electron-hole wave function overlap (b) for structures containing GaN, AlGan, and AlInN barriers.

AlGaN barriers show a shift of more than 30 nm in the same range of currents. Due to the large φ_{pz} and thus an increased $|\Delta\varphi_{tot}|$ across the QW, $|\langle\psi_e|\psi_h\rangle|^2$ is reduced for all cases as shown in Fig. 6(b) in comparison to Fig. 4(b). Despite this fact, however, the wave function overlap for the InGaN/AlInN structure is still nearly three times larger than for designs containing GaN and AlGaN barriers. Values in the range of 10%–25% are calculated for structures with GaN and AlGaN barriers, whereas LEDs containing AlInN show values of 45%–60%. These results indicate that AlInN is a promising barrier material to be used in high performance yellow LED structures.

In summary, we studied semi-polar $(11\bar{2}2)$ InGaN-based LEDs for blue (450 nm) and yellow (560 nm) emission using GaN, AlGaN, and AlInN as barrier materials. In comparison to GaN and AlGaN, structures with AlInN show a good color stability and higher electron-hole wave function overlaps. Wavelength shifts lower than 10 and 20 nm and the wave function overlap higher than 90% and 40% were calculated for emission at 450 and 560 nm, respectively. Although a large built-in electric potential drop is expected for QWs with GaN and AlGaN barriers under applied bias, it is not necessarily the case for the system containing AlInN. Here, a large spontaneous polarization of the barrier material counteracts the piezoelectric polarization and the external electric potential. As a result, the total built-in electric field inside the QW can be controlled by composition engineering of the AlInN barrier and the InGaN active region. Finally, we show that the polarization matching method used for *c*-plane III-nitrides can be optimized for any growth orientation.

This work was supported by the European Union Project ALIGHT (No. FP7-280587). S.S. also acknowledges financial support from the Science Foundation Ireland under Project No. 10/IN.1/I2994.

[1]S. Nakamura, MRS Bull. **34**, 101 (2009).
[2]T. Takeuchi, C. Wetzel, S. Yamaguchi, H. Sakai, H. Amano, I. Akasaki, Y. Kaneko, S. Nakagawa, Y. Yamaoka, and N. Yamada, Appl. Phys. Lett. **73**, 1691 (1998).
[3]T. Wunderer, P. Brückner, B. Neubert, F. Scholz, M. Feneberg, F. Lipski, M. Schirra, and K. Thonke, Appl. Phys. Lett. **89**, 041121 (2006).
[4]J.-H. Ryou, W. Lee, J. Limb, D. Yoo, J. P. Liu, R. D. Dupuis, Z. H. Wu, A. M. Fischer, and F. A. Ponce, Appl. Phys. Lett. **92**, 101113 (2008).
[5]T. Detchprohm, M. Zhu, S. You, L. Zhao, W. Hou, Ch. Stark, and Ch. Wetzel, Proc. SPIE **7954**, 79540N-1 (2011).
[6]Y.-R. Wu, Y.-Y. Lin, H.-H. Huang, and J. Singh, J. Appl. Phys. **105**, 013117 (2009).
[7]S. Schulz and E. P. O'Reilly, Appl. Phys. Lett. **99**, 223106 (2011).
[8]M. H. Kim, M. F. Schubert, Q. Dai, J. K. Kim, E. F. Schubert, J. Piprek, and Y. Park, Appl. Phys. Lett. **91**, 183507 (2007).
[9]M. A. Caro, S. Schulz, S. B. Healy, and E. P. O'Reilly, J. Appl. Phys. **109**, 084110 (2011).
[10]F. Scholz, Semicond. Sci. Technol. **27**, 024002 (2012).
[11]H. Masui, S. Nakamura, S. P. DenBaars, and U. K. Mishra, IEEE Trans. Electron Devices **57**, 88 (2010).
[12]Y. Zhao, S. Tanaka, C.-C. Pan, K. Fujito, D. Feezell, J. S. Speck, S. P. DenBaars, and S. Nakamura, Appl. Phys. Express **4**, 082104 (2011).
[13]C. C. Pan, S. Tanaka, F. Wu, Y. Zhao, J. S. Speck, S. Nakamura, S. P. DenBaars, and D. Feezell, Appl. Phys. Express **5**, 062103 (2012).
[14]Y. Zhao, Q. Yan, C. Y. Huang, S. C. Huang, P. S. Hsu, S. Tanaka, C. C. Pan, Y. Kawaguchi, K. Fujito, C. G. Van de Walle, J. S. Speck, S. P. DenBaars, S. Nakamura, and D. Feezell, Appl. Phys. Lett. **100**, 201108 (2012).
[15]Y. Zhao, S. H. Oh, F. Wu, Y. Kawaguchi, S. Tanaka, K. Fujito, J. S. Speck, S. P. DenBaars, and S. Nakamura, Appl. Phys. Express **6**, 062102 (2013).
[16]A. Strittmatter, J. E. Northrup, N. M. Johnson, M. V. Kisin, P. Spiberg, H. El-Ghoroury, A. Usikov, and A. Syrkin, Phys. Status Solidi B **248**, 561 (2011).
[17]V. F. Mymrin, K. A. Bulashevich, N. I. Podolskaya, I. A. Zhmakin, S. Yu. Karpov, and Yu. N. Makarov, Phys. Status Solidi C **2**, 2928 (2005).
[18]P. G. Moses, M. Miao, Q. Yan, and C. G. Van de Walle, J. Chem. Phys. **134**, 084703 (2011).
[19]M. A. Caro, S. Schulz, and E. P. O'Reilly, Phys. Rev. B **88**, 214103 (2013).
[20]E. Sakalauskas, H. Behmenburg, C. Hums, P. Schley, G. Rossbach, C. Giesen, M. Heuken, H. Kalisch, R. H. Jansen, J. Bläsing, A. Dadgar, A. Krost, and R. Goldhahn, J. Phys. D: Appl. Phys. **43**, 365102 (2010).
[21]S. Schulz, M. A. Caro, L.-T. Tan, P. J. Parbrook, R. W. Martin, and E. P. O'Reilly, Appl. Phys. Express **6**, 121001 (2013).
[22]A. E. Romanov, T. J. Baker, S. Nakamura, and J. S. Speck, J. Appl. Phys. **100**, 023522 (2006).
[23]G. Verzellesi, D. Saguatti, M. Meneghini, F. Bertazzi, M. Goano, G. Meneghesso, and E. Zanoni, J. Appl. Phys. **114**, 071101 (2013).
[24]Y. C. Shen, G. O. Mueller, S. Watanabe, N. F. Gardner, A. Munkholm, and M. R. Krames, Appl. Phys. Lett. **91**, 141101 (2007).